Interfacial adhesion quality in 3D printed continuous CF/PA6 composites at filament/matrix and interlaminar scales

Fabienne Touchard, Laurence Chocinski-Arnault, Teddy Fournier, Christophe Magro, Antoine Lafitte, Amélie Caradec

Interfacial adhesion quality in 3D printed continuous CF/PA6 composites at filament/matrix and interlaminar scales

Fabienne TOUCHARD[1*], Laurence CHOCINSKI-ARNAULT[1], Teddy FOURNIER[2], Christophe MAGRO[2], Antoine LAFITTE[1], Amélie CARADEC[1]

[1]*Institut PPRIME, CNRS-ENSMA-Université de Poitiers, Département Physique et Mécanique des Matériaux, ENSMA, 1, Av. Clément Ader, B.P. 40109, 86961 Futuroscope Cedex, France*

[2]*Centre Technologique Nouvelle-Aquitaine Composites & Matériaux Avancés, Bât Cheminnov – ENSCBP 16 avenue Pey Berland 33600 PESSAC, France*

*: corresponding author: fabienne.touchard@ensma.fr

Abstract:

Fused deposition modelling (FDM) is a promising additive manufacturing technology for the fabrication of continuous fibre reinforced thermoplastic composites. However, a major concern is the performances of the interfacial bonding in these composites. The aim of this study is to evaluate the interface quality of a 3D printed carbon/PA6 composite at two scales: the filament/matrix scale and the interlaminar one. Two different types of samples were made: monofilament composites for performing fragmentation tests, and double cantilever beam (DCB) samples for realising mode I interlaminar fracture tests. After measuring the strength of the individual carbon filament, the fragment lengths were observed by micro-CT and measured in monofilament composites in order to calculate the interfacial shear strength (*IFSS*). The DCB tests allowed the determination of the interlaminar fracture toughness (G_{Ic}) for 0°//0° and +45°//-45° interfaces. The obtained results are promising for such 3D printed composites.

Keywords: Additive manufacturing ; fused filament fabrication ; fragmentation ; delamination

1. Introduction

Continuous fibre reinforced polymer (FRP) composites are widely used in aerospace, marine and automotive industries owing to their high performance to weight ratio. They are traditionally manufactured by manual lay-up, resin transfer moulding, pultrusion or filament winding. However these methods imply long production time, elevated costs and frequently the need for moulds [1]. Therefore, there is a growing interest in the new processes based on additive manufacturing, as the fused deposition modelling (FDM) technology. This method has several advantages: (i) it allows the printing of complex geometric patterns without the need of secondary machining operation, (ii) its flexibility allows rapid prototyping and opens the way to customized parts, (iii) it reduces material wastage and it is relatively low cost [2]. FDM technology allows creating 3D geometries depositing layer by layer extruded filament. The most frequently used filaments are thermoplastic ones, as PLA (polylactide) [3], ABS (acrylonitrile butadiene styrene) [4] or nylon [5]. In order to improve mechanical performance of 3D printed parts, fibres have been added in polymers. Development of short fibre reinforced polymer composites made by additive manufacturing has been on-going for about a decade [6]. For example, the addition of short glass or carbon fibres allows the enhancement of pure polymer strength [7-10]. However, the load-bearing capacity of short fibre reinforced polymer composites is still limited. Recent research trends are thus in the direction of developing new 3D printed composites including continuous fibres. Fabrication of composites with continuous carbon, glass, Kevlar or natural fibres have been performed [11-13]. Some authors have evaluated the mechanical properties of 3D printed continuous fibre composites, such as tensile and compressive properties [14,15], tensile and flexural properties [1,11,16], impact properties [17], fatigue and creep properties [18]. It is important to notice that, during the printing procedure, no pressure is applied after a layer is laid up. Therefore, there are unfilled spaces in the material. These voids and pores, inherently present in the matrix, affect the mechanical properties of the 3D printed composites [13,19]. Moreover, the additive manufacturing may lead to poorer interfacial properties as compared to the ones of conventional composites [20]. Indeed, the deposition of side-by-side filaments and the layer-by-layer method may have a detrimental impact on the adhesion quality at filament/matrix interface

and may be responsible for degradation of interlaminar fracture toughness [21,22]. Although interface quality at the two scales, filament/matrix and interlaminar scales, is a key-parameter for mechanical performance of 3D printed continuous fibre composites, there is little data available on these aspects. Barile et al. have performed delamination tests using 3D printed double cantilever beam (DCB) specimens, made with bulk polymer (ABS) [23]. Garcia-Guzman et al. [24] have studied resistance of adhesive joints in glass/nylon DCB specimens with structured interface. Concerning 3D printed carbon/nylon composites, He et al. [19] have compared the Mode I interlaminar fracture toughness (G_{Ic}) values at 0°//0° interface using DCB samples with or without a post compression moulding process. Nevertheless, to the best of authors' knowledge, there are no published results concerning the adhesion quality at filament/matrix interface and at multidirectional interlaminar interface in 3D printed continuous fibre composites. The aim of the current study is to bridge this gap.

The studied material is a continuous carbon/nylon composite, elaborated by additive manufacturing based on fused deposition modelling method. Carbon reinforcement was chosen, rather than glass or Kevlar ones, because of its high mechanical properties [25,26]. In order to analyse the carbon/nylon interface, specific 3D printed monofilament composites are manufactured. Fragmentation tests are performed and micro-CT observations are realised. The interfacial shear strength (*IFSS*) value is determined for characterising the interface between the carbon filament (CF) and the PA6 matrix. Delamination behaviour at 0°//0° and +45°//-45° interfaces is characterised by testing 3D printed DCB samples. The effect of the stacking sequence on mode I delamination resistance is investigated and R-curves are analysed.

2. Materials and methods

2.1 3D printer and materials

All specimens used in this study were fabricated using a desktop 3D printer: the MarkTwo® developed by Markforged®. It uses its own software designated Eiger®. It can print two kinds of material independently and, hence, it has two extruders and two print heads. One of the print head is used to print the matrix and the other one to print fibre reinforcement. The design of the 3D printer allows

continuous fibre reinforcement to be placed as required through the layer-by-layer deposition process. All samples were printed with a nylon filament and a carbon filament (CF) supplied by Markforged®. Nylon and carbon fibre (reinforcement) layers were printed with hot end temperatures of 265°C, on a non-heated print bed. The pre-set layer height was chosen equal to 125μm. The matrix-only filament, constituted by bulk PA6, was 1.75mm in diameter. The carbon filament comes in spools and is composed of multiple strands of carbon fibres coated with a thermoplastic polymer. The carbon filament diameter was measured to be 375±18μm (Fig. 1). The carbon fibre weight fraction of this filament is about 40% [14,19]. Table 1 gives the tensile characteristics of single carbon fibres [27, 28] and PA6 polymer [29].

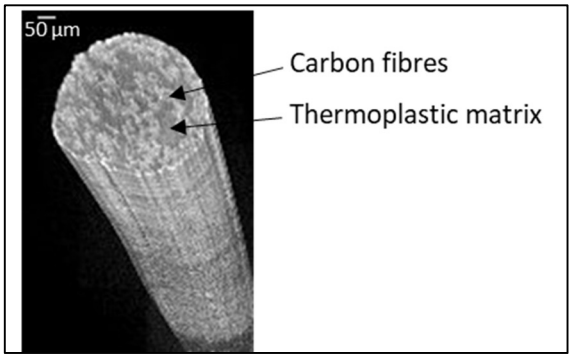

Fig. 1. Micro-CT 3D view of the as-received carbon filament (CF).

Table 1. Average tensile characteristics of single carbon fibres [27,28] and PA6 polymer [29].

	Tensile strength (MPa)	**Tensile modulus (GPa)**
Single carbon fibre [27,28]	4000	238
PA6 [29]	51	1.7

The fibre reinforcement fill type is configured in the Eiger® software, which can have an isotropic or concentric fibre-laydown pattern. The term “isotropic” does not define the mechanical properties of the specimen. Isotropic reinforcement allows a unidirectional pattern that can be rotated at each layer. The concentric reinforcement allows a concentric ring pattern of the carbon filament and deposits a free number of rings depending on the specimen geometry. Each type of reinforcement fill has to be chosen according to the desired geometry [20,21].

2.2 Monofilament composites

Fragmentation tests on monofilament composites allow investigating the interface quality between the reinforcement and the matrix. When applying a tensile loading to monofilament composites, the load is transferred through the matrix into the filament by means of shear stress at the interface. Filament failure occurs when this transferred stress reached the tensile strength of the filament. The filament will continue to fracture into shorter length fragments as the load increases, until the filament fragments are so small that the tensile stresses induced in the filament can no longer reach the filament tensile strength. At this point, a state of saturation is reached and the fragmentation process ceases. Fragmentation tests have been widely used at the scale of single fibre [30-35], or at the scale of yarn [36,37]. For 3D printed composites, the interesting scale is the carbon filament one. Therefore, 3D printed carbon/nylon samples with only one filament of carbon aligned in the loading direction and centered in the specimens were manufactured. The concentric fill type was used in order to produce required parts, with a central rectangular hole (Fig. 2). At first, eight layers of nylon were deposited (Fig. 2a), then a layer with a central ring of carbon filament was laid down (Fig. 2b), and finally eight other nylon layers were deposited.

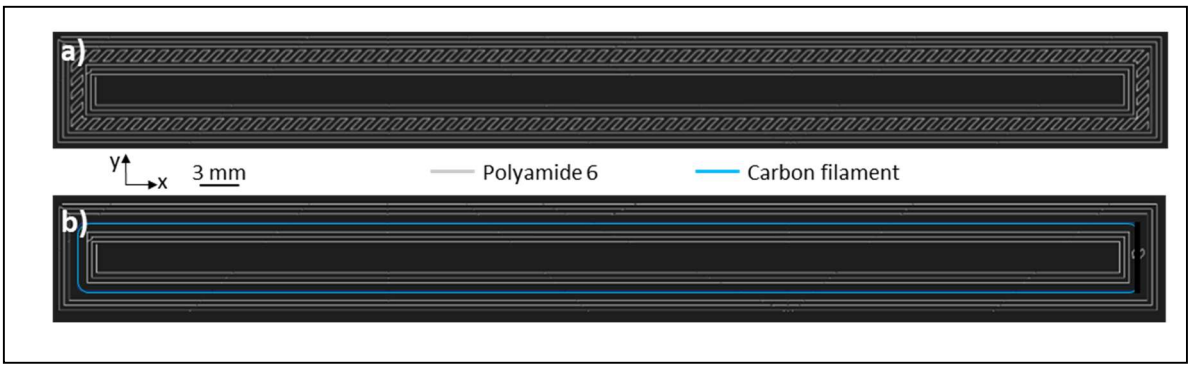

Fig. 2. The 3D printed layer fill configurations a) for the nylon layers, b) for the layer with the carbon filament (the grey line represents the nylon filament and the blue line is for the carbon filament).

It led to rectangular parts 91.2mm long, 9.1mm wide and 2.25mm thick, in which four monofilament composite samples could be cut (Fig.3a). Three rectangular parts were printed, resulting in twelve monofilament composite samples. Each monofilament composite sample used for fragmentation test had dimensions of 45mm×3mm×2.25mm, with a gauge length of 15mm (Fig. 3b).

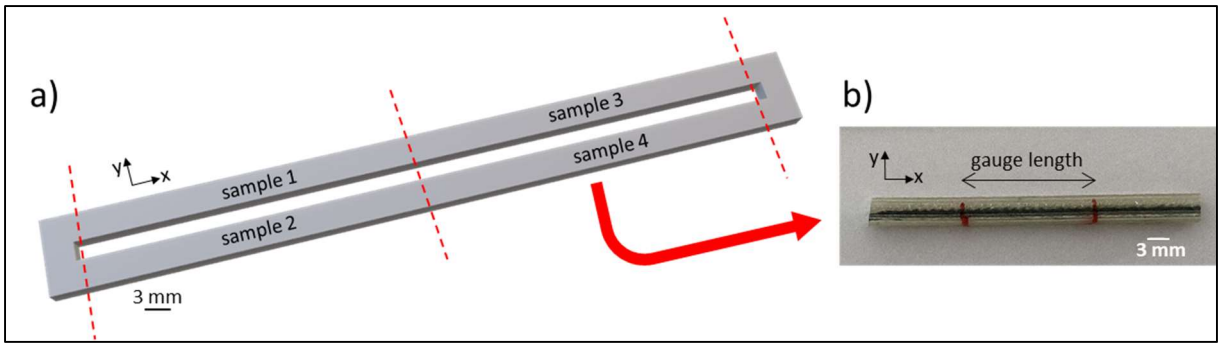

Fig. 3. a) Geometry of the printed rectangular part, b) a monofilament composite sample.

2.3 DCB specimens

The Mode I interlaminar behaviour of the 3D printed CF/nylon composites has been investigated by testing DCB specimens. The design of the stacking sequence of DCB coupons has to be carefully chosen. First of all, the two sublaminates on either side of the delaminated interface should have identical stiffness, so that the delamination propagates in pure mode I conditions [38]. For this reason, the pre-crack is positioned in the midplane of the laminate. Standard test methods for mode I concern only delamination initiation for unidirectional composites, while laminates widely used in industrial applications are multidirectional [39,40]. Therefore, two different stacking sequences have been studied in this work, in order to analyse two interfaces: the 0°//0° interface and the +45°//-45° interface. Four layers with carbon filament were deposited in each specimen, i.e. two composite layers on each side of the delamination plane. The other twenty layers were made with pure nylon filament. The fibre orientation and layer arrangement were specified using Eiger® software, based on the isotropic fill type. The additive manufacturing process was interrupted in order to place the 45µm thick nonadhesive insert at the midplane of the coupon (Fig. 4).

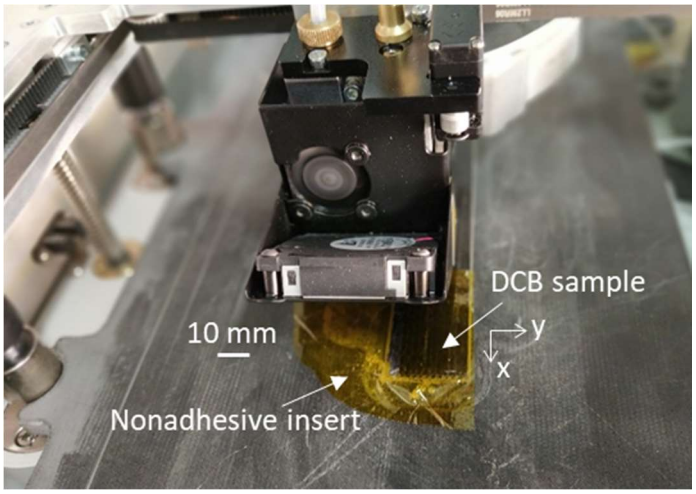

Fig. 4. 3D printing of DCB samples, with the addition of the nonadhesive insert.

For the 0°//0° specimens, the fibre layers were placed at 0° with respect to the axial direction, and for the +45°//-45° ones, the carbon layers had +45° and -45° with respect to the axial direction. Nylon and fibre layers were laid down horizontally, layer by layer, to complete the specimens (Fig. 5). Final geometry of the 3D printed DCB samples was 125mm long, 25mm wide and 3mm thick. Piano hinge tabs were then adhesively bonded to specimens following EN6033 standard [41]. The length a_0 of the initial crack was 40±1mm. Both edges of the DCB coupons were polished using fine sandpaper and white paint was applied to the sides of the specimens in order to help the visual detection of the crack tip.

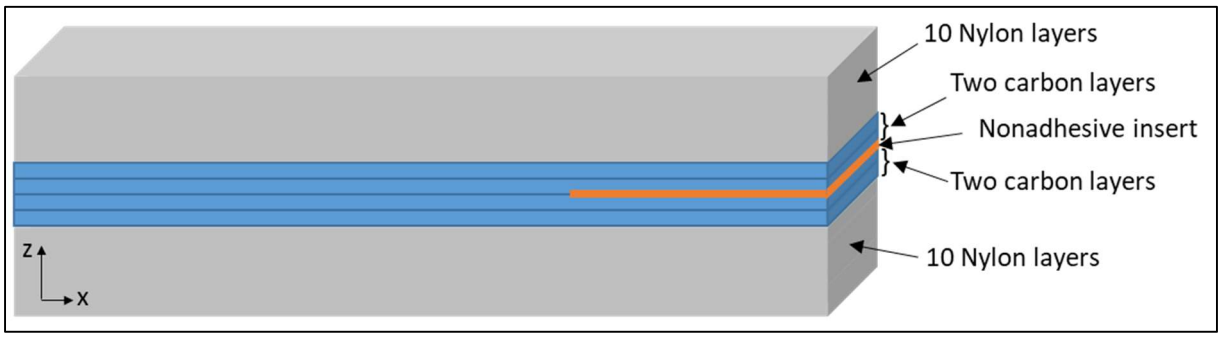

Fig. 5. Scheme of DCB samples with the different layers (sketch not to scale).

2.4 Mechanical tests

All the samples were tested at room temperature using an INSTRON 1195 machine with a load cell of 2000N. The testing machine was equipped with manual screw action grips. During each test, the time, the load and the crosshead displacement were recorded through the acquisition system of the machine.

2.4.1 Filament tensile testing

A tensile characterisation of the as-received carbon filaments was carried out by performing tests at a crosshead speed of 5mm/min. The gauge length of the tested carbon filaments was 20mm. 80 grit sand papers were used in the jaws to improve clamping.

2.4.2 Fragmentation tests

The fragmentation tests were performed on monofilament composite samples at a rather high loading rate (75mm/min) in order to reach the fragmentation saturation level despite the PA6 ductility. For these samples, sand papers were also used in the jaws (Fig. 6).

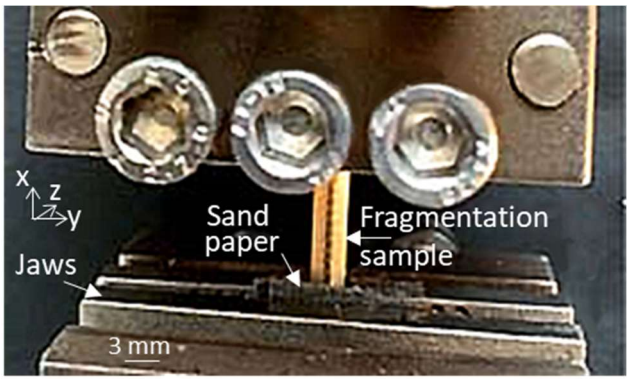

Fig. 6. Fragmentation test on a monofilament carbon/PA6 sample.

2.4.3 DCB tests

DCB specimens were loaded at a constant displacement rate of 5mm/min. The extremities of piano hinge tabs were tightened into the grips of the testing machine. An incremental test method was applied [42]. Each DCB specimen was loaded until the propagation of the delamination was of about 5mm. The cross-head was then stopped, the specimen was unloaded and loaded again. The delamination extension process was then repeated until the final delamination length reached approximately 85mm. The minimum force at unloading was chosen to be equal to 0.5N in order to avoid compression of the specimen. The position of the crack was measured using a graduated scale drawn directly on the specimen itself. The crack tip propagation was recorded in situ during tests with a digital camera (Fig. 7).

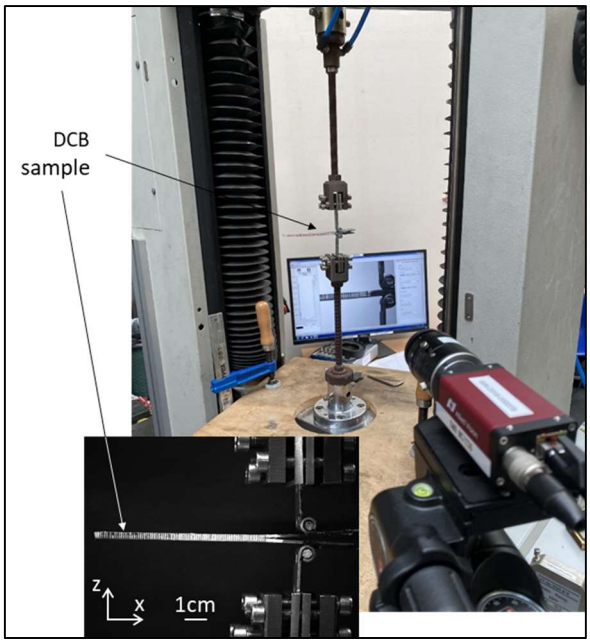

Fig. 7. Experimental set-up for interlaminar tests, with a digital camera for delamination tip recording.

2.5 Micro-CT

Micro-CT observations were performed using an UltraTom CT scanner manufactured by RX Solution (France). The system consists in a Hamamatsu micro focus sealed X-ray tube operating at 20-150kV/0-500 µA, within a maximum power of 75W. X-rays, generated by the source, diverge at an angle providing a cone-beam. Various geometric magnifications can thus be obtained by moving the sample close to the source to provide high resolution mode or close to the detector to provide low resolution measurements. The generator and the detector are also mobile to cover a large range of magnification. A 5µm resolution was used in this work. The 3D reconstruction was performed using an algorithm based on the filtered back-projection procedure for Feldkamp cone beam geometry.

3. Results and discussion

3.1 Tensile properties of the carbon filament

The as-received carbon filament was tested in tension before using it for the composite 3D printing. The examples of tensile curves obtained for three samples are plotted in Fig. 8. The measured characteristics are given in Table 2.

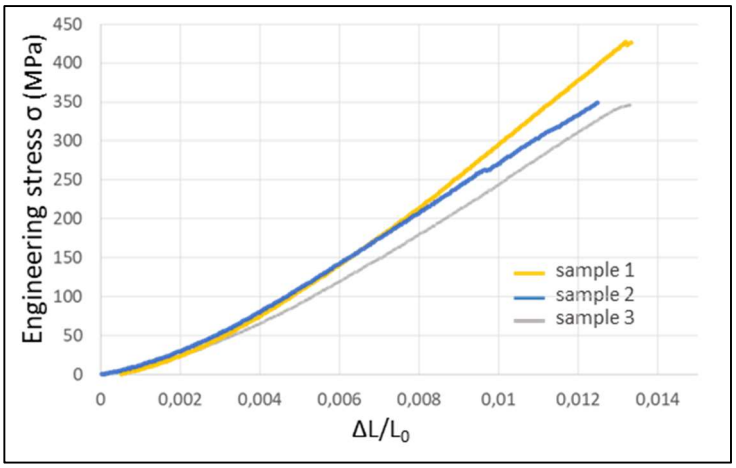

Fig. 8. Tensile curves for three samples of the as-received carbon filament.

Table 2. Tensile characteristics of the as-received carbon filament.

	Gauge length (mm)	Strength (MPa)	Apparent modulus (GPa)	Strain at failure (%)
Carbon filament (CF)	20 ± 1	399 ± 54	31.8 ± 2.5	1.32 ± 0.07

The strength of the carbon filament was determined equal to 399±54MPa. This value is much lower than the strength values of single carbon fibres, which are about 4000MPa [27,28]. This is due to the fact that the carbon filament is a strand made of about 1000 individual fibres and impregnated with a thermoplastic polymer [43]. The values of the modulus and the strain at failure given in Table 2 were determined from the machine crosshead displacement. They must therefore be considered with caution. Nevertheless, the modulus of the carbon filament is also much lower than the single carbon fibre one, which is about 238GPa, while the strain at failure is of the same order [28]. The tensile strength value measured for the as-received carbon filament was used for the calculation of the interfacial shear strength (*IFSS*) values.

3.2 Characterisation of the filament/matrix interface

Fragmentation tests were performed on monofilament CF/PA6 composites. Then, micro-CT observations were realised on tested samples. Fig. 9 shows for example three different micro-CT views

of a fragmented sample. The longitudinal view (Fig. 9a) allows to see a part of the sample gauge length, with the carbon filament located in the middle of the nylon matrix. An entire filament fragment can be observed, and the fragment length l_f can be measured between the two fragmentations.

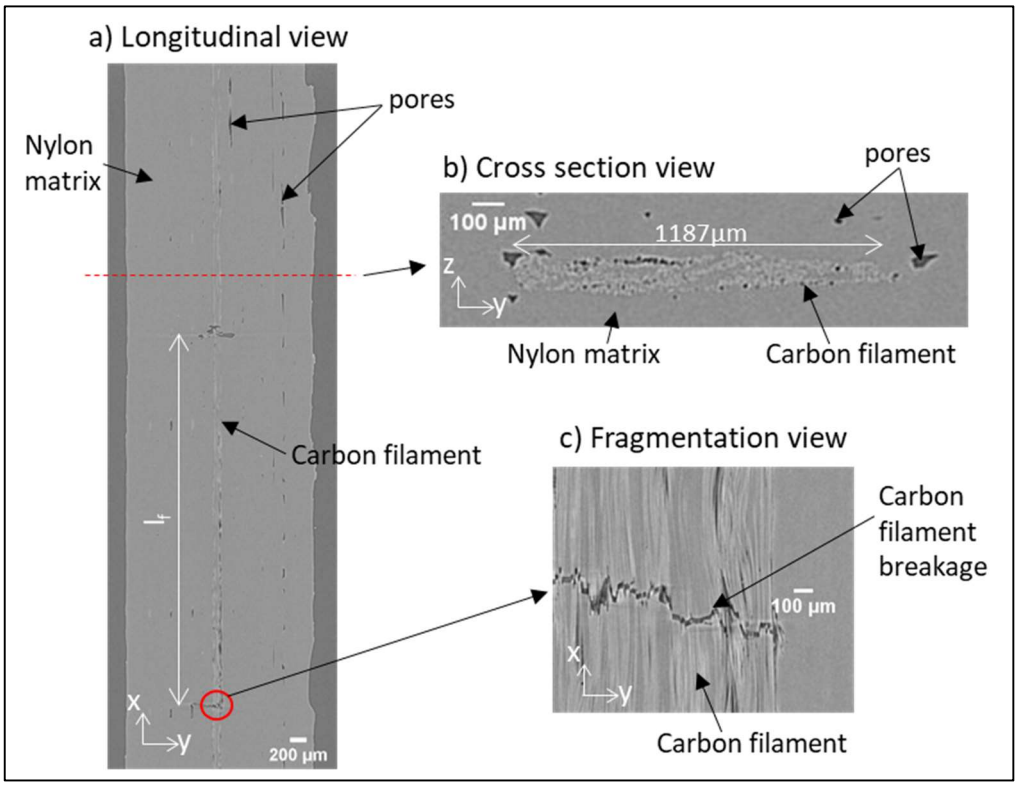

Fig. 9. Micro-CT observation of a fragmented monofilament carbon/PA6 sample: a) longitudinal view, b) cross section view, and c) fragmentation view.

The cross section view (Fig. 9b) shows the section of the carbon filament, made of several fibres, embedded in the nylon matrix. It can be seen that the carbon filament is no more circular. Indeed, during the manufacturing, the filament is heated, enabling it to pass through the extruder orifice. On the way it is laid up, it is cooled and progressively solidified. The filament is thus subjected to its own weight, and to the weight of next layers. Therefore, its initial circular section becomes a flattened section (Fig. 9b). Moreover, some pores with a characteristic triangular shape can be seen in Fig. 9b. These triangular voids have already been observed in 3D printed materials and are commonly found between adjacent filaments [6]. Fig. 9c focuses on a fragmentation of the carbon filament. It clearly shows that the CF breakage is made of successive failures of individual carbon fibres, describing a sort of staircase.

Measurements of the length of all the obtained CF fragments were performed. Then, the critical fragment length was calculated using equation 1 [44]:

$$l_c = \frac{4}{3} \cdot \overline{l_f} \quad (1)$$

where $\overline{l_f}$ is the average value of the fragment length. The critical fragment length value reflects the stress transfer efficiency between the filament and the matrix at the interface. According to Kelly and Tyson [45], the interfacial shear strength value (*IFSS*) may be estimated using equation 2:

$$IFSS = \frac{\sigma_f(l_c) \cdot d}{2 \cdot l_c} \quad (2)$$

where d is the filament diameter, l_c is the critical fragment length and $\sigma_f(l_c)$ is the filament strength for a length equal to the critical filament length. Due to the impossibility to determine directly the tensile strength of a carbon filament with a length equal to the critical fragment length, an extrapolation of strength at critical length l_c can be done by using the Weibull cumulative distribution function. Using the two-parameter Weibull distribution, the strength value for critical length can be determined by equation 3 [46,47]:

$$\sigma_f(l_c) = \sigma_f(L_0) \left(\frac{L_0}{l_c}\right)^{\frac{1}{m}} \quad (3)$$

where m is the shape parameter of Weibull distribution, l_c is the critical fragment length and $\sigma_f(L_0)$ is the strength value for the gauge length L_0. In our case, L_0 and $\sigma_f(L_0)$ are given in Table 2. Concerning the parameter m, we made the assumption that its value is similar for carbon filament and for carbon fibre. All the values are reported in Table 3.

Table 3. Critical fragment length, shape parameter of Weibull distribution for carbon fibres (*: from [48]), strength value of the filament for critical length, and *IFSS* value for single filament carbon/PA6 samples.

Critical fragment length (mm)	m	σ_f (l_c) (MPa)	IFSS (MPa)
4.75 ± 0.25	7.4*	485 ± 70	19.9 ± 5.2

The obtained interfacial shear strength value (*IFSS*) for the CF/PA6 interface is 19.9±5.2MPa (Table 3). This value cannot be compared with literature ones, because, to the best of authors' knowledge, there is no paper yet dealing with fragmentation tests for 3D printed composites. Nevertheless, it is possible to compare it with the *IFSS* value obtained for carbon/PA6 samples manufactured by molding process. Zhu et al. [49] prepared single fibre composites made of carbon fibre embedded in PA6 matrix. Thanks to fragmentation tests, they determined an *IFSS* value of 18.53±4MPa. It is thus possible to deduce that the adhesion quality of the carbon/PA6 interface is very similar for 3D printed composites in comparison with classical molded composites. Therefore, the presence of pores does not seem to deteriorate the overall quality of adhesion at the interface between the carbon filament and the nylon matrix. This result is very promising for this new type of process.

3.3 Interlaminar properties

DCB specimens with two different stacking sequences were tested in order to determine the interlaminar fracture toughness values for 3D printed carbon/PA6 composites. Fig. 10 shows crack tip views for the two types of DCB specimens: with 0°//0° interface and with +45°//-45° interface. Some fibre bridging can be observed, as it has been reported for example for glass/polyester [42] or carbon/epoxy [50] laminates. When it is of high intensity, the fibre bridging can substantially elevate the measured fracture resistance. But for the tested samples, fibre bridging was not very significant (Fig. 10).

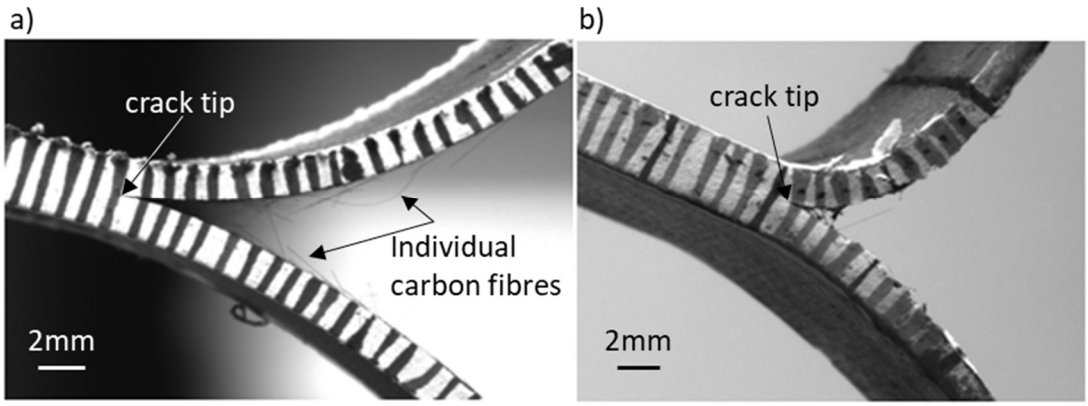

Fig. 10. Crack tip view during interlaminar tests: a) for 0°//0° interface, and b) for +45°//-45° interface.

The load-displacement curves obtained for one sample of each configuration are plotted in Fig. 11. It can be noticed that the shape of the curves for the two orientations is quite different. This is due to the large permanent deformation remaining after unloading in the case of the +45°//-45° interface. It indicates that significant plastic deformation has occurred for this orientation. This phenomenon has already been observed for conventional composites [42]. The interlaminar fracture toughness values (G_{Ic}) were determined according to the EN6033 standard [41] by using equation 4:

$$G_{Ic} = \frac{\Delta E}{w.\Delta a} \tag{4}$$

where ΔE is the energy to achieve the propagated crack length, w is the width of the specimen and Δa is the propagated crack length. For each load drop, ΔE was obtained by computing the area of the loop, and Δa was calculated by subtracting the position of the crack tip after and before the drop [38].

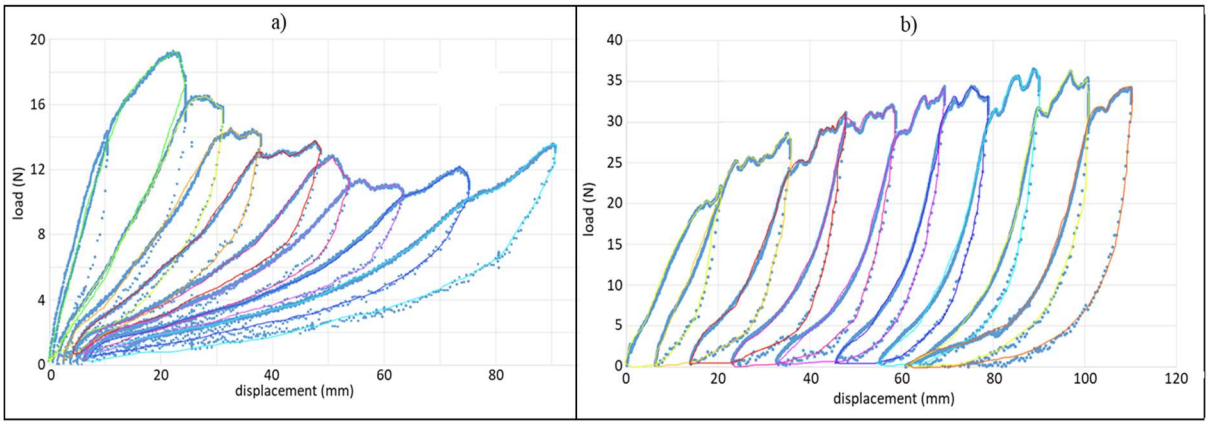

Fig. 11. Load-displacement curves of DCB specimens: a) for 0°//0° interface, and b) for +45°//-45° interface.

The obtained R-curves are plotted in Fig. 12. R-curves show the evolution of the resistance to delamination propagation as a function of the delamination length. For the 0°//0° interface, it can be seen that the G_{Ic} value remains relatively constant, around 1228J/m^2 (Fig. 12a). For the +45°//-45° interface, R-curves show a significant increase in the values, occurring for a delamination length of 10mm for one sample (sample 1), and for a length of 20mm for the other one (sample 2) (Fig. 12b).

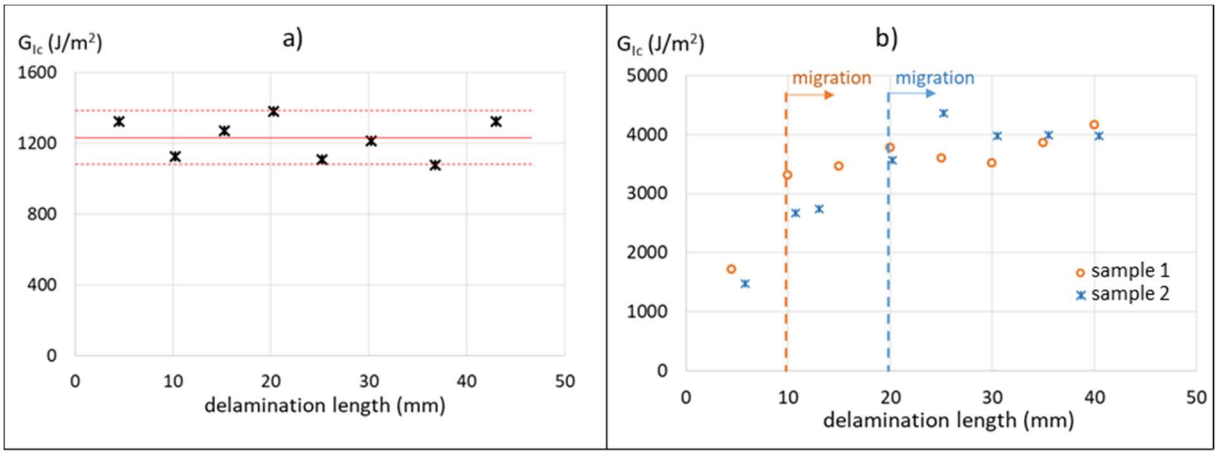

Fig. 12. R-curves for Mode I interlaminar fracture toughness of 3D printed carbon/PA6 composites: a) for 0°//0° interface, and b) for +45°//-45° interface.

The observation of the fracture surfaces for samples with +45°//-45° interface (Fig. 13) has shown that a migration of the delamination from one layer to the other occurred after a few loading-unloading

cycles. This phenomenon of migration during delamination propagation is well-known and only G_{Ic} values measured before the migration must be taken into account [50].

Fig. 13. Fracture surface of a DCB sample with +45°//-45° interface: observation of the delamination migration from one layer to the other.

Finally, the G_{Ic} values determined for the two tested configurations are given in Table 4. For the 0°//0° interface, the obtained value can be compared with the one determined by He et al. [19] for a 3D printed carbon/PA6 composite. They determined a G_{Ic} value equal to 1467±20J/m^2. Our value is quite similar - slightly lower - despite the very different methodology used (different 3D printer parameters, different lay-ups, different DCB tests, different calculation of G_{Ic}). Concerning the +45°//-45° interface, there is no published data for 3D printed composites. But it can be noted that for a carbon/epoxy made from prepregs, the G_{Ic} value determined for the +45°//-45° interface was also significantly higher than the one for the 0°//0° interface [38]. It tends to validate the G_{Ic} results obtained for the carbon/nylon composite. However, other tests with other stacking sequences are necessary to better understand the interlaminar behaviour of the 3D printed composites.

Table 4. Mode I interlaminar fracture toughness values determined from DCB tests on 3D printed CF/PA6 composites.

	Interface 0°//0°	**Interface +45°//-45°**
G_{Ic} (J/m^2)	1228 ± 114	2150 ± 525

4. Conclusion

The interface bonding performances of 3D printed continuous carbon fibre reinforced nylon composites were evaluated in this study. Interfacial properties were investigated at two different scales: at the filament/matrix scale and at the interlaminar one. Preliminary tensile tests were performed on the as-received carbon filament, in order to determine its mechanical characteristics. Then, monofilament composites were manufactured by using the concentric fill type, with only one filament of carbon aligned in the loading direction. Fragmentation tests were realised on these monofilament composites and micro-CT observations were made after failure. Thanks to the measurement of fragment lengths, the interfacial shear strength value (*IFSS*) was determined. Results show that the obtained value is quite similar to that of classical molded carbon/PA6 composites. DCB samples were also manufactured by FDM technique. Two stacking sequences were studied, in order to analyse two different interfaces: 0°//0° and +45°//-45°. For the latter, a migration phenomenon was observed and only the first points of the corresponding R-curves were used. Finally, the obtained results are quite promising. Future work is necessary to analyse the interface bonding quality of these composites in different configurations. Nevertheless, these results give a database that can be useful for further industrial developments of 3D printed continuous composites, in particular to enrich finite element models for designing optimised structures.

Acknowledgements:

This work was partially funded by the French Government program “Investissements d'Avenir” (EQUIPEX GAP, reference ANR-11-EQPX-0018) and by the CPER FEDER project of Région Nouvelle Aquitaine. It pertains to the French Government program “Investissements d’Avenir” (EUR INTREE, reference ANR-18-EURE-0010).

References:

[1] Goh GD, Dikshit V, Nagalingam AP, Goh GL, Agarwala S, Sing SL, Wei J, Yeong WY. Characterization of mechanical properties and fracture mode of additively manufactured carbon fiber

and glass fiber reinforced thermoplastics. Materials & Design 2018;137:79-89, https://doi.org/10.1016/j.matdes.2017.10.021.

[2] Wickramasinghe S, Do T , Tran P. FDM-Based 3D Printing of Polymer and Associated Composite: A Review on Mechanical Properties, Defects and Treatments, Polymers 2020;12(7):1529, DOI: 10.3390/polym12071529.

[3] Ezeh OH, Susmel L. On the notch fatigue strength of additively manufactured polylactide (PLA). Int. J. of Fatigue 2020;136:105583, https://doi.org/10.1016/j.ijfatigue.2020.105583.

[4] Ameri B, Taheri-Behrooz F, AlihaMRM. Fracture loads prediction of the modified 3D-printed ABS specimens under mixed-mode I/II loading. Eng. Fracture Mechanics 2020;235:107181, https://doi.org/10.1016/j.engfracmech.2020.107181.

[5] Terekhina S, Skornyakov I, Tarasova T, et al. Effects of the infill density on the mechanical properties of nylon specimens made by filament fused fabrication. Technologies 2019;7(3):57, DOI: 10.3390/technologies7030057.

[6] Goh GD, Yap YL, Agarwala S, Yeong WY. Recent progress in additive manufacturing of fiber reinforced polymer composite. Advanced Materials Technologies 2019;4(1):1800271, DOI: 10.1002/admt.201800271.

[7] Dickson AN, Abourayana HM, Dowling DP. 3D printing of fibre-reinforced thermoplastic composites using fused filament fabrication-A review. Polymers 2020;12(10):2188, DOI: 10.3390/polym12102188.

[8] Wang P, Zou B, Ding S, Huang C, Shi Z, Ma Y, Yao P. Preparation of short CF/GF reinforced PEEK composite filaments and their comprehensive properties evaluation for FDM-3D printing. Comp. Part B: Engineering 2020;198:108175, https://doi.org/10.1016/j.compositesb.2020.108175.

[9] Ivey M, Melenka GW, Carey JP, Ayranci C. Characterizing short-fiber-reinforced composites produced using additive manufacturing. Advanced Manufacturing-Polymer & Composites Science 2017;3(3):81-91, DOI: 10.1080/20550340.2017.1341125.

[10] Sodeifian G, Ghaseminejad S, Yousefi AA. Preparation of polypropylene/short glass fiber composite as Fused Deposition Modeling (FDM) filament. Results in Physics 2019;12:205-222, https://doi.org/10.1016/j.rinp.2018.11.065.

[11] Dickson AN, Barry JN, McDonnell KA, Dowling DP. Fabrication of continuous carbon, glass and Kevlar fibre reinforced polymer composites using additive manufacturing. Additive Manufacturing 2017;16:146-152, DOI: 10.1016/j.addma.2017.06.004.

[12] Yeong WY, Goh GD. 3D printing of carbon fiber composite: the future of composite industry? Matter 2020;2(6):1361-1363, 2020, DOI: 10.1016/j.matt.2020.05.010.

[13] Melenka GW, Cheung BKO, Schofield JS, Dawson MR, Carey JP. Evaluation and prediction of the tensile properties of continuous fiber-reinforced 3D printed structures. Composite Structures 2016;153:866-875, DOI: 10.1016/j.compstruct.2016.07.018.

[14] Justo J, Tavara L, Garcia-Guzman L, Paris F. Characterization of 3D printed long fibre reinforced composites. Composite Structures 2018;185:537-548, DOI: 10.1016/j.compstruct.2017.11.052.

[15] van der Klift F, Koga Y, Todoroki A, Ueda M, Hirano Y, Matsuzaki R. 3D printing of continuous carbon fibre reinforced thermo-plastic (CFRTP) tensile test specimens. Open Journal of Composite Materials 2016;6:18-27, DOI: 10.4236/ojcm.2016.61003.

[16] Yao XH, Luan CC, Zhang DM, Lan LJ, Fu JZ. Evaluation of carbon fiber-embedded 3D printed structures for strengthening and structural-health monitoring. Materials & Design 2017;114:424-432, DOI: 10.1016/j.matdes.2016.10.078.

[17] Caminero MA, Chacon JM, Garcia-Moreno I, Rodriguez GP. Impact damage resistance of 3D printed continuous fibre reinforced thermoplastic composites using fused deposition modelling. Composites Part B-Engineering 2018;148:93-103, DOI: 10.1016/j.compositesb.2018.04.054.

[18] Mohammadizadeh M, Imeri A, Fidan I, Elkelany M, 3D printed fiber reinforced polymer composites - Structural analysis. Composites Part B: Engineering 2019;175:107112, https://doi.org/10.1016/j.compositesb.2019.107112.

[19] He Q, Wang H, Fu K, Ye L. 3D printed continuous CF/PA6 composites: Effect of microscopic voids on mechanical performance. Composites Science and Technology 2020;191:108077, https://doi.org/10.1016/j.compscitech.2020.108077.

[20] Araya-Calvo M, Lopez-Gomez I, Chamberlain-Simon N, Leon-Salazar JL, Guillen-Giron T, Corrales-Cordero JS, Sanchez-Brenes O. Evaluation of compressive and flexural properties of continuous fiber fabrication additive manufacturing technology. Additive Manufacturing 2018;22:157-164, DOI: 10.1016/j.addma.2018.05.007.

[21] Caminero MA, Chacon JM, Garcia-Moreno I, Reverte JM. Interlaminar bonding performance of 3D printed continuous fibre reinforced thermoplastic composites using fused deposition modelling. Polymer Testing 2018;68:415-423, DOI: 10.1016/j.polymertesting.2018.04.038.

[22] Liu YT, Song HY, Yao TT, Zhang W, Zhu H, Wu GP. Effects of carbon nanotube length on interfacial properties of carbon fiber reinforced thermoplastic composites. J. of Materials Science 2020;55(32):15467-15480, DOI: 10.1007/s10853-020-05129-w.

[23] Barile C, Casavola C, Cazzato A. Acoustic emissions in 3D printed parts under mode I delamination test. Materials 2018;11(9):1760, DOI: 10.3390/ma11091760.

[24] Garcia-Guzman L, Tavara L, Reinoso J, Justo J, Paris F. Fracture resistance of 3D printed adhesively bonded DCB composite specimens using structured interfaces: Experimental and theoretical study. Composite Structures2018;188:173-184, DOI: 10.1016/j.compstruct.2017.12.055.

[25] van de Werken N, Tekinalp H, Khanbolouki P, Ozcan S, Williams A, Tehrani M. Additively manufactured carbon fiber-reinforced composites: State of the art and perspective. Addit. Manuf. 2020;31:100962. https://doi.org/10.1016/j.addma.2019.100962.

[26] Chacón JM, Caminero MA, Núñez PJ, García-Plaza E, García-Moreno I, Reverte JM. Additive manufacturing of continuous fibre reinforced thermoplastic composites using fused deposition modelling: Effect of process parameters on mechanical properties. Composites Science and Technology, 2019;181:107688, https://doi.org/10.1016/j.compscitech.2019.107688.

[27] Wang ML, Bian WF. The relationship between the mechanical properties and microstructures of carbon fibers. New Carbon Materials 2020;35(1):42-49, DOI: 10.1016/S1872-5805(20)60474-7.

[28] Yao JW, Yu WD, Pan D. Tensile strength and its variation of PAN-based carbon fibers. III. weak-link analysis. J. of Applied Polymer Science 2008;110(6):3778-3784, DOI: 10.1002/app.24879.

[29] Markforged, Material datasheet, REV 4.0 - 12/01/2020 [online] https://www-objects.markforged.com/craft/materials/composites-data-sheet.pdf [accessed May 2020]

[30] Seghini MC, Touchard F, Sarasini F, Cech V, Chocinski-Arnault L, Mellier D, Tirillò J, Bracciale MP, Zvonek M. Engineering the interfacial adhesion in basalt/epoxy composites by plasma polymerization. Comp Part A 2019;122:67-76, https://doi.org/10.1016/j.compositesa.2019.04.013.

[31] Mahato B, Babarinde VO, Abaimov SG, Lomov SV, Akhatov I. Interface strength of glass fibers in polypropylene: Dependence on the cooling rate and the degree of crystallinity. Polymer Composites 2019;41(4), doi:10.1002/pc.25456.

[32] Yang S, Liu W, Fang Y, Huo R. Influence of hygrothermal aging on the durability and interfacial performance of pultruded glass fiber-reinforced polymer composites. Journal of Materials Science 2018;54(1), doi:10.1007/s10853-018-2944-6.

[33] Kim JH, Kwon DJ, Shin PS, Park HS, Baek YM, DeVries KL, Park JM. Evaluation of interfacial and mechanical properties of glass fiber and p-DCPD composites with surface treatment of glass fiber. Composites Part B: Engineering 2018;153:420-428, https://doi.org/10.1016/j.compositesb.2018.09.007.

[34] Sugimoto Y, Shimamoto D, Imai Y, Hotta Y. Simultaneous evaluation of tensile strength and interfacial shear strength of short length carbon fibers using fragmentation test. Carbon 2020;161: 83-88, DOI: 10.1016/j.carbon.2019.12.089.

[35] Liu YT, Song HY, Yao TT, Zhang WS, Zhu H, Wu GP. Effects of carbon nanotube length on interfacial properties of carbon fiber reinforced thermoplastic composites. J. of Materials Science 2020;55(32):15467-15480, DOI: 10.1007/s10853-020-05129-w.

[36] Guillebaud-Bonnafous C, Vasconcellos D, Touchard F, Chocinski-Arnault L. Experimental and numerical investigation of the interface between epoxy matrix and hemp yarn. Composites Part A 2012;43:2046–2058. http://dx.doi.org/10.1016/j.compositesa.2012.07.015.

[37] Seghini MC, Touchard F, Sarasini F, Chocinski-Arnault L, Mellier D, Tirillò J. Interfacial adhesion assessment in flax/epoxy and in flax/vinylester composites by single yarn fragmentation test: correlation with micro-CT analysis. Comp. Part A 2018;113:66–75. https://doi.org/10.1016/j.compositesa.2018.07.015.

[38] Daghia F, Cluzel C. The climbing drum peel test: an alternative to the double cantilever beam for the determination of fracture toughness of monolithic laminates. Composites Part A 2015;78:70-83, DOI: 10.1016/j.compositesa.2015.07.010.

[39] Shokrieh MM, Heidari-Rarani M, Ayatollahi MR. Delamination R-curve as a material property of unidirectional glass/epoxy composites. Materials & Design 2012;34:211-218, DOI: 10.1016/j.matdes.2011.08.006.

[40] Schon J, Nyman T, Blom A, Ansell H. A numerical and experimental investigation of delamination behaviour in the DCB specimen. Composites Science and Technology 2000;60(2):173-184, DOI: 10.1016/S0266-3538(99)00113-X.

[41] EN6033 – 2015 – Aerospace series. Carbon fibre reinforced plastics. Test method. Determination of interlaminar fracture toughness energy. Mode I. GIc.

[42] Ozdil F, Carlsson LA. Beam analysis of angle-ply laminate DCB specimens. Composites Science and Technology 1999;59(2):305-315, DOI: 10.1016/S0266-3538(98)00069-4.

[43] Pascual-Gonzalez C, Iragi M, Fernandez A, Fernandez-Blazquez JP, Aretxabaleta L, Lopes CS. An approach to analyse the factors behind the micromechanical response of 3D-printed composites. Composites Part B-Engineering 2020;186:107820, DOI: 10.1016/j.compositesb.2020.107820.

[44] Ohsawa T, Nakayama A, Miwa M, Hasegawa A. Temperature dependence of critical fiber length for glass fiber - reinforced thermosetting resins. J. Appl. Polym. Sci. 1978;22:3203–3212. DOI: 10.1002/app.1978.070221115.

[45] Kelly A, Tyson WR. Tensile properties of fibre-reinforced metals: Copper/tungsten and copper/molybdenum. J. Mech. Phys. Solids 1965, 13:329–350, DOI: 10.1016/0022-5096(65)90035-9.

[46] Seghini MC, Touchard F, Sarasini F, Chocinski-Arnault L, Tirillò J, Bracciale MP, Zvonek M, Cech V. Effects of oxygen and tetravinylsilane plasma treatment on mechanical and interfacial

properties of flax yarns in thermoset matrix composites. Cellulose 2020;27:511–530, DOI: 10.1007/s10570-019-02785-3.

[47] Zafeiropoulos NE. On the use of single fibre composites testing to characterize the interface in natural fibre composites. Compos. Interfaces 2007;14:807–820, DOI: 10.1163/156855407782106438.

[48] Ramirez FA, Carlsson LA, Acha BA. Evaluation of water degradation of vinylester and epoxy matrix composites by single fiber and composite tests. J Mater Sci 2008;43:5230–5242, https://doi.org/10.1007/s10853-008-2766-z.

[49] Zhu P, Shi J, Bao LM. Effect of polyetherimide nanoparticle coating on the interfacial shear strength between carbon fiber and thermoplastic resins. Applied Surface Science 2020;509:145395, DOI: 10.1016/j.apsusc.2020.145395.

[50] Rehan MSB, Rousseau J, Fontaine S, Gong XJ. Experimental study of the influence of ply orientation on DCB mode-I delamination behavior by using multidirectional fully isotropic carbon/epoxy laminates. Composite Structures 2017;161:1-7, DOI: 10.1016/j.compstruct.2016.11.036.

Figure captions:

Fig. 1. Micro-CT 3D view of the as-received carbon filament (CF).

Fig. 2. The 3D printed layer fill configurations a) for the nylon layers, b) for the layer with the carbon filament (the grey line represents the nylon filament and the blue line is for the carbon filament).

Fig. 3. a) Geometry of the printed rectangular part, b) a monofilament composite sample.

Fig. 4. 3D printing of DCB samples, with the addition of the nonadhesive insert.

Fig. 5. Scheme of DCB samples with the different layers (sketch not to scale).

Fig. 6. Fragmentation test on a monofilament carbon/PA6 sample.

Fig. 7. Experimental set-up for interlaminar tests, with a digital camera for delamination tip recording.

Fig. 8. Tensile curves for three samples of the as-received carbon filament.

Fig. 9. Micro-CT observation of a fragmented monofilament carbon/PA6 sample: a) longitudinal view, b) cross section view, and c) fragmentation view.

Fig. 10. Crack tip view during interlaminar tests: a) for 0°//0° interface, and b) for +45°//-45° interface.

Fig. 11. Load-displacement curves of DCB specimens: a) for 0°//0° interface, and b) for +45°//-45° interface.

Fig. 12. R-curves for Mode I interlaminar fracture toughness of 3D printed carbon/PA6 composites: a) for 0°//0° interface, and b) for +45°//-45° interface.

Fig. 13. Fracture surface of a DCB sample with +45°//-45° interface: observation of the delamination migration from one layer to the other.

Tables:

Table 1. Average tensile characteristics of single carbon fibres [27,28] and PA6 polymer [29].

	Tensile strength (MPa)	**Tensile modulus (GPa)**
Single carbon fibre [27,28]	4000	238
PA6 [29]	51	1.7

Table 2. Tensile characteristics of the as-received carbon filament.

	Gauge length (mm)	**Strength (MPa)**	**Apparent modulus (GPa)**	**Strain at failure (%)**
Carbon filament (CF)	20 ± 1	399 ± 54	31.8 ± 2.5	1.32 ± 0.07

Table 3. Critical fragment length, shape parameter of Weibull distribution for carbon fibres (*: from [44]), strength value of the filament for critical length, and *IFSS* value for single filament carbon/PA6 samples.

Critical fragment length (mm)	**m**	**σ_f (l_c) (MPa)**	**IFSS (MPa)**
4.75 ± 0.25	7.4*	485 ± 70	19.9 ± 5.2

Table 4. Mode I interlaminar fracture toughness values determined from DCB tests on 3D printed CF/PA6 composites.

	Interface 0°//0°	**Interface +45°//-45°**
G_{Ic} (J/m^2)	1228 ± 114	2150 ± 525